Climate Dynamics (2019) 52:4227–4245
https://doi.org/10.1007/s00382-018-4377-y

The role of air–sea interactions in regulating the thermal effect of the Tibetan–Iranian Plateau on the Asian summer monsoon

Bian He[1,2,3] · Yimin Liu[1,3] · Guoxiong Wu[1,3] · Ziqian Wang[1,4] · Qing Bao[1]

Received: 1 May 2017 / Accepted: 31 July 2018 / Published online: 4 August 2018

Abstract

The thermal effect of the Tibetan–Iranian Plateau (TIP) on the Asian summer monsoon and the role of air–sea interactions over the Indian Ocean in regulating the effects of the TIP are explored. The results demonstrate that the direct thermal effect of the TIP produces a lower troposphere cyclonic circulation in the area surrounding the TIP and increases the continental precipitation over South and East Asia. It also decreases the precipitation over the tropical Indian Ocean and increases the sea-surface temperature (SST) of the tropical Indian Ocean with a large gradient zone located along 10°N but decreases SST of the western coast of Indonesia. In the lower troposphere, the air–sea interaction induced by the TIP thermal forcing produces an anticyclonic circulation surrounding the TIP and a stronger westerly flow to the south of the anticyclone. A circulation dipole thus forms to the south of the TIP. Together with this horizontal dipole, a meridional circulation dipole is generated to the south of the TIP, which is characterized by strong air ascent from 10 to 15°N where a strong westerly flow occurs, and the descent of air over the southern slope of the TIP and south Hemisphere. These results demonstrate that the indirect effect of the air–sea interaction over the Indian Ocean induced by the TIP thermal forcing is to counteract its direct effect on the Asian summer monsoon. The uncertainty of this indirect effect is also discussed.

Keywords Air–sea interactions · Asian summer monsoon · Tibetan–Iranian Plateau · Topographical heating

1 Introduction

The Tibetan Plateau (TP), the largest highland in the world, is located in the central and eastern parts of the Eurasian continent and has a strong effect on the climate of Asia (Manabe and Terpstra 1974; Tao and Ding 1981; Huang 1985; Zhao and Chen 2001; Wu et al. 2007, 2012a; Wang et al. 2008; Zhou et al. 2009; Liu et al. 2012; Boos and Kuang 2010, 2013). During the boreal winter, atmospheric circulations are mainly modulated by the mechanical forcing of the TP (Queney 1948; Bolin 1950; Yeh 1950), which can excite gravity waves and Rossby waves and is important in the development of stationary waves during the northern winter (Charney and Eliassen 1949; Held et al. 2002). During the boreal summer, the TP has been found to be a heat source (Flohn 1957; Yeh et al. 1957) closely linked to the onset, formation and evolution of the Asian summer monsoon (ASM) (Wu and Zhang 1998, Hsu and Liu 2003; Duan and Wu 2005; Liu et al. 2007; Wu et al. 2012b). Based on station records, Ye and Gao (1979) found that the increase in atmospheric heating over the TP during the boreal summer is dominated by vertical diffusive heating from the surface

Electronic supplementary material The online version of this article (doi:https://doi.org/10.1007/s00382-018-4377-y) contains supplementary material, which is available to authorized users.

✉ Yimin Liu
lym@lasg.iap.ac.cn

✉ Guoxiong Wu
gxwu@lasg.iap.ac.cn

[1] State Key Laboratory of Numerical Modeling for Atmospheric Sciences and Geophysical Fluid Dynamics (LASG), Institute of Atmospheric Physics (IAP), Chinese Academy of Sciences, Beijing 100029, China

[2] Key Laboratory of Meteorological Disaster of Ministry of Education, Nanjing University of Information Science and Technology, Nanjing 210044, China

[3] University of Chinese Academy of Sciences, Beijing 100029, China

[4] School of Atmospheric Sciences, and Guangdong Province Key Laboratory for Climate Change and Natural Disaster Studies, Sun Yat-sen University, Guangzhou 510275, China

of the TP. Subsequently, Wu et al. (1997, 2007) suggested that the sensible heating on the slope surface of the TP is the major driving force in the transport of abundant water vapor from the ocean surface to the land, leading to monsoonal precipitation over the Asian continent, known as the sensible heat-driven air pump (SHAP).

In recent decades, the effects of the TP on atmospheric circulations have been investigated through simulation with atmospheric general circulation models (AGCMs) and coupled GCMs (CGCMs). By comparing a simulation with mountains to one without mountains in an AGCM with a prescribed sea-surface temperature (SST), Hahn and Manabe (1975) found that the presence of the TP is instrumental in maintaining the South Asian low-pressure system, leading to high temperatures in the middle and upper troposphere over the TP, causing the monsoon climate to extend farther north, with similar results found using different models (Xu et al. 2009, 2010). More detailed topographic experiments have been carried out by Kitoh (2004, 2010), who assessed the effects of different mountain heights in a CGCM and found that the ASM precipitation moves gradually inland when forced by progressive mountain uplift. In this scenario, the Pacific subtropical anticyclone and the associated trade winds also become stronger. These studies emphasized the importance of the high elevation of the TP on maintaining the ASM. Notably, Wu et al. (2007) documented that the thermal forcing of the TP is more important than the mechanical forcing in maintaining the ASM. Through a series of sensitivity experiments involving changes in topographic and thermal conditions, they determined that sensible heating on sloping lateral surfaces appears to be the major source of the forcing. The warm ascending air that develops over the TP in the summer pulls air from below, and the lower tropospheric air from the surrounding areas converges on the TP region before climbing the heated sloping surfaces. Moreover, Wu et al. (2012b) showed that, in addition to the thermal effect of the TP, the thermal effect of the Iranian Plateau (IP) is also important in maintaining the ASM. Sensible heating of the IP causes a cyclonic anomaly in the lower troposphere and transports a large amount of water vapor from the Arabian Sea (AS) to northern India, which favors intense monsoonal precipitation. Therefore, the thermal effects of the TP and the IP should be considered as an integral part of the large-scale topographic forcing affecting the dynamics of the Asian monsoon (Wu et al. 2012b).

Despite these efforts, our understanding of the thermal effect of the TP on the ASM remains insufficient, since most of the sensitivity experiments used a prescribed SST, and the Tibetan–Iranian Plateau (TIP) heating effect on the SST was not considered. Meanwhile, using CGCMs, several studies (Kitoh 1997, 2004, 2010; Okajima and Xie 2007; Koseki et al. 2008) have shown that the TP significantly influences the SST and the associated changes in the Asian climate. Abe et al. (2003) revealed that the SST in the equatorial Indian Ocean increases with mountain uplift, resulting in increase of local precipitation. This increase is caused by the ocean surface dynamics due to the enhanced monsoonal circulation. Kitoh (2004) demonstrated that mountain uplift results in an increased SST within the western tropical Pacific and the Maritime Continent, and a decreased SST within the western Indian Ocean and the central subtropical Pacific in the summertime. Abe et al. (2013) examined the effects of the presence of the TP on the onset of the ASM using both CGCMs and AGCMs, and found that the onset of the South Asian summer monsoon in the presence of the TP is strongly related to the air–sea interactions during the pre-monsoon season. The lower SST seen in the AS in the presence of the TP is related to the later onset of summer monsoonal precipitation in South Asia, while the heat transport in the mixed layer is responsible for changes in the SST in the absence of the TP. Using a regional model, Wang et al. (2018) found TP heating could cool the SST over northern Indian Ocean by enhancing southwestly winds. Despite these studies, the responses of the SST and the associated changes in the mixed layer to the uplifted thermal effects of the TP remain unclear. Therefore, it is important to analyze changes in the mixed layer to investigate the impacts of the thermal forcing associated with the TIP on the subsurface Indian Ocean. To address these issues, it is necessary to carry out thermal sensitivity experiments with CGCMs.

The thermal effects of the TIP on the formation of the ASM are re-evaluated here, and the associated air–sea interactions are analyzed through comparison of sensitivity experiments performed with a CGCM and an AGCM. Section 2 introduces the datasets and models, the experiment design, and the model evaluation. Section 3 presents the direct influence of the TIP heating on the ASM based on the CGCM simulations. Section 4 presents the direct influence of the thermal effect of the TIP on the circulation and thermal status of the Indian Ocean. Section 5 discusses the role of air–sea interactions in modulating the thermal effect of the TIP on the ASM, which is the so-called indirect influence of the thermal effect of the TIP on the ASM. The uncertainty of such an indirect influence is evaluated in Sect. 6. Finally, the conclusion and discussion are presented in Sect. 7.

2 Datasets, model, experiment design, and model evaluation

2.1 Datasets

The precipitation data were derived from the Global Precipitation Climatology Project (GPCP) monthly mean dataset (Adler et al. 2003), which is constructed on a 2.5° × 2.5°

grid over the globe and covers the period from 1979 to the present. This dataset is available at http://www.esrl.noaa.gov/psd/data/gridded/data.gpcp.html.

The multilevel air temperature, specific humidity, and wind field from the European Centre for Medium-range Weather Forecasts (ECMWF) ERA-Interim (Dee et al. 2011) were used. The dataset includes a 1.5° × 1.5° grid resolution and covers the period from 1979 to the present and is available at http://apps.ecmwf.int/datasets/.

2.2 Model

The Flexible Global Ocean-Atmosphere-Land System Model spectral version 2 (FGOALS-s2) was used here as the climate system model, and was composed of four individual components: version 2 of the spectral atmospheric model (SAMIL2) developed at the State Key Laboratory of Numerical Modeling for Atmospheric Sciences and Geophysical Fluid Dynamics, Institute of Atmospheric Physics (LASG/IAP) (Wu et al. 1996; Bao et al. 2010), version 2 of the LASG/IAP Climate system Ocean Model (LICOM2) (Liu et al. 2013), version 3 of the Community Land Model (CLM3) (Oleson et al. 2004), and version 5 of the Community Sea Ice Model (CSIM5) (Briegleb et al. 2004). The fluxes were exchanged between these components using version 6 of the coupler module from the National Center for Atmospheric Research (Collins et al. 2006). The basic performance of FGOALS-s2 is described in Bao et al. (2013).

2.3 Experiment design

To investigate the direct and indirect influence of the thermal effect of the TIP on the ASM and the associated air–sea interactions, we conducted a series of experiments as summarized in Table 1. The first experiment (CON) was performed using FGOALS-s2. The CGCM model was integrated over 90 years, with results for the last 50 years analyzed. The second experiment (TIPNS) was the same as the CON experiment, but the TIP surface was not allowed to heat the atmosphere. That is, in integrating the atmospheric thermodynamic equation, the vertical diffusion heating at the surface was set to zero during the summer months (June–July–August) for grid points within the region extending from 30° to 110°E and from 10° to 45°N with elevations above 500 m. This method is the same as that used in Wu et al. (2012b) and He et al. (2015). In addition, two AGCM experiments (CON_OBSST and TIPNS_OBSST) were carried out using the SAMIL2 component, which used the same setting as the CON and TIPNS runs, except that the SST and sea ice were forced by the observed climatological monthly mean. The AGCM was integrated over 30 years, and the mean values for the last 20 years were analyzed.

The direct influence of the TIP thermal forcing was estimated by calculating the differences between the CON and TIPNS experiments and between the CON_OBSST and TIPNS_OBSST experiments. We calculated the changes in the total sensible heat flux for the AGCM and CGCM using the method described in Ma et al. (2014), with the resulting values of 172 and 178 TW, respectively (Table 1). Student's *t*-test was also applied to assess the statistical significance of the model results.

To investigate the indirect influence of the TIP thermal forcing, two additional pairs of AGCM experiments CON_CPSST, TIPNS_CPSST, CON_NSSST, and TIPNS_NSSST were carried out (Table 1). In the CON_CPSST and TIPNS_CPSST experiments, the SST outputs from the CON experiments were archived and employed to replace the observed SST in CON_OBSST and TIPNS_OBSST as

Table 1 Experiment design

Name	Description
CON	Climate Model Intercomparison Project experiment using the external forcings prescribed as their climatological values. The model is integrated for 90 years, and the mean values from the last 50 years are analyzed
TIPNS	The same as for the CON experiment, but the surface sensible heating is not allowed to heat the atmosphere during June–July–August over the domain (30°–110°E/10°–45°N) where the TIP topography is above 500 m. The change of total sensible heat flux is 178 TW
CON_OBSST	Atmospheric Model Intercomparison Project run using the observed climatological SST and sea ice at the lower boundary. The other forcing fields are prescribed as their climatological values. The model is integrated for 30 years, and the mean values from the last 20 years are analyzed
TIPNS_OBSST	As for the CON_OBSST experiment, but the surface sensible heating is not allowed to heat the atmosphere during June–July–August over the domain (30°–110°E/10°–45°N), where the TIP topography is above 500 m. The change of the total sensible heat flux is 172 TW
CON_CPSST	Same as the CON_OBSST experiment, but the SST is prescribed by outputs from the CON experiment
TIPNS_CPSST	Same as the TIPNS_OBSST experiment, but the SST is prescribed by outputs from the CON experiment
CON_NSSST	Same as the CON_OBSST experiment, but the SST is prescribed by outputs from the TIPNS experiment
TIPNS_NSSST	Same as the TIPNS_OBSST experiment, but the SST is prescribed by outputs from the TIPNS experiment

the lower boundary condition. Similarity, in CON_NSSST and TIPNS_NSSST, the SST outputs from TIPNS were prescribed. In other words, the AGCM experiments are driven by the SST generated from the corresponding CGCM, and not by the observed SST. Thus, the indirect effect of TIP thermal forcing was evaluated by comparing the difference between a pair of CGCM experiments with and without the surface sensible heating over the TIP and a pair of AGCM experiments with the same experimental settings, which can be expressed as

$$\mathrm{DD\_CPSST} = (\mathrm{CON}-\mathrm{TIPNS}) - (\mathrm{CON\_CPSST}-\mathrm{TIPNS\_CPSST}) \quad (1)$$

or

$$\mathrm{DD\_NSSST} = (\mathrm{CON}-\mathrm{TIPNS}) - (\mathrm{CON\_NSSST}-\mathrm{TIPNS\_NSSST}) \quad (2)$$

It is noteworthy that this method is a little different to the methods presented in previous literature (Kitoh 2004; Okajima and Xie 2007), which used the observed SST to force the AGCM model to estimate the indirect effect of the mountain. The different approach was taken because the indirect effect can be largely isolated from the influence of the SST difference between the CGCM and the observations by using the SST from the CGCM. However, it is widely known that CGCMs suffer from SST simulation bias. To evaluate the influence of this kind of bias on the indirect effect, we also estimated the indirect effect of TIP thermal forcing by using the traditional method:

$$\mathrm{DD\_OBS} = (\mathrm{CON}-\mathrm{TIPNS}) - (\mathrm{CON\_OBSST}-\mathrm{TIPNS\_OBSST}). \quad (3)$$

The common features derived from these results are confirmed as the TIP indirect effect on the ASM based on the modeling efforts, and their differences and associated SST biases are also discussed in detail in Sect. 6.

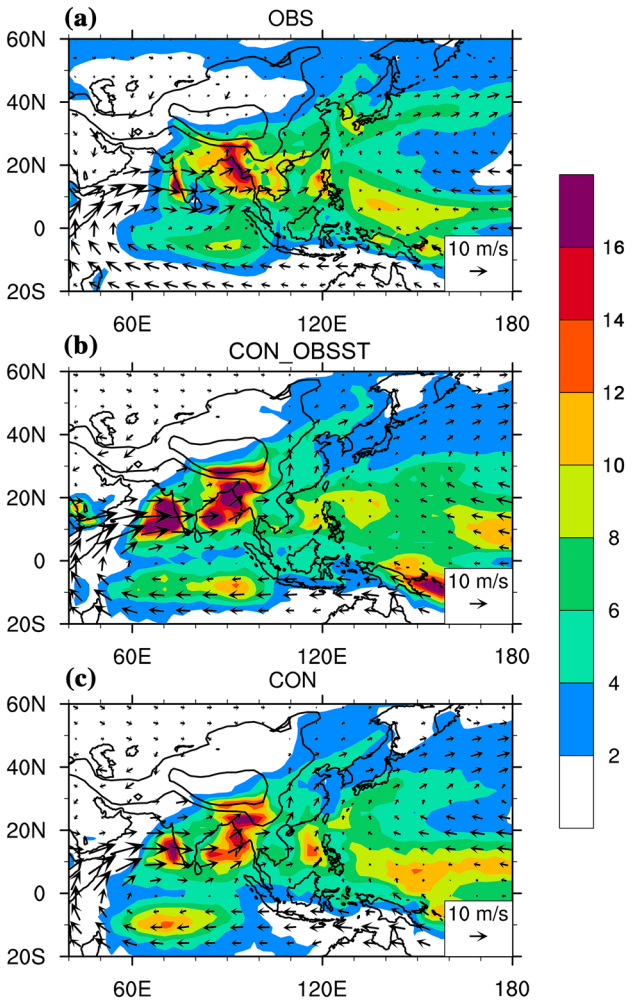

Fig. 1 Climate mean June–July–August precipitation (shaded, mm day^{-1}) and 850-hPa wind speed (vector, m s^{-1}) from **a** reanalysis data (1979–2008), with precipitation from the GPCP dataset and wind speed from ERA-Interim Reanalysis, and from the numerical experiments **b** CON_OBSST and **c** CON. The black contours denote elevations of 1000 and 3000 m, respectively

2.4 Model evaluation

The performance of the model in capturing the basic pattern of the ASM was evaluated first, with the simulated precipitation and lower tropospheric wind speed produced by the CON_OBSST run shown in Fig. 1b. Compared with the observational data (Fig. 1a), the CON_OBSST run captures the main features of the ASM precipitation pattern, with more than 4 mm day^{-1} of rainfall covering the area over the Indian Ocean, the Asian continent, and the western Pacific Ocean, while also simulating the maximum precipitation center over the eastern AS, the Bay of Bengal (BOB), and the southern slope of the TP. The Somali Jet, the monsoonal trough over the BOB, and the anticyclone over the western Pacific are also well simulated. However, the model underestimates the precipitation over northern New Guinea and overestimates the precipitation over the AS, the BOB, and the southern slope of the TP. Moreover, the simulated rain belt over the western Pacific is located to the north of that seen in the observational data. The overall monsoonal features simulated in the CON experiment (Fig. 1c) are consistent with those simulated in the CON_OBSST run. There were a series of improvements from the use of the CGCM. First, the simulated precipitation pattern over the western Pacific in the CON run is more realistic and closer to the observations. Moreover, the centers of maximum precipitation in the AS, the BOB, and the southern slope of the TP are weaker in the CON run than in the CON_OBSST run and are also more consistent with the observations. The above evaluation demonstrates that FGOALS-s2 and its atmospheric component SAMIL2 are capable of capturing the major characteristics

of the ASM and can be used for the following sensitivity experiments.

3 Direct influence of the thermal effect of the Tibetan–Iranian Plateau on the Asian summer monsoon

We first investigate the response of the ASM to topographic heating in the CGCM. For this purpose, the surface sensible heating over the TIP is removed and the result (TIPNS) is shown in Fig. 2a, and then compared with its counterparts in the control experiment. Compared with Figs. 1c, 2a shows a similar pattern of the ASM over the ocean even if the thermal effect of the TIP is removed, which is consistent with previous studies (Hahn and Manabe 1975; Xu et al. 2009; Wu et al. 2012b) and shows that the large-scale, land–sea thermal contrast is of fundamental importance for the formation of the tropical ASM. However, in the sensitivity experiment, the monsoonal rain belt barely extends over the Asian continent, and the East Asian monsoon is significantly weakened.

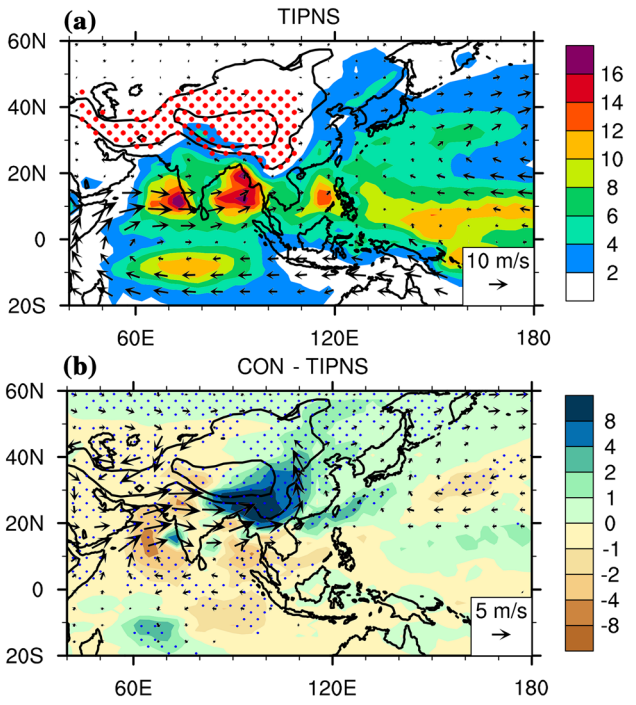

Fig. 2 June–July–August mean precipitation (shaded, mm day^{-1}) and 850-hPa wind speed (vector, m s^{-1}) produced by the numerical experiments **a** TIPNS, and the differences **b** between the CON and TIPNS experiments. The red dots in **a** denote the regions where the sensible heating was modified. The vectors and blue dots in **b** denote the winds and precipitation difference passing the 95% significance in the *t*-test respectively. The black contours denote elevations of 1000 and 3000 m, respectively

To examine the direct thermal impacts of the TIP on changes in the ASM in the lower troposphere, we show the precipitation and 850-hPa wind differences between the CON and TIPNS runs (Fig. 2b). The thermal effect of the TIP causes increased precipitation over the southern slope of the TP and the East Asian continent, and decreased precipitation over central Asia, and almost the entire Indian Ocean. The increase in monsoonal precipitation over the Asian continent is also accompanied by cyclonic circulation around the TIP in the lower troposphere. The direct effects on precipitation, i.e. changes in precipitation are similar over the Asian continent, but different over the Indian Ocean and the western Pacific between the CGCM (Fig. 2b) and AGCM results (Fig. S2c in OSM), implying that air–sea interaction may play significant roles in modulating the TIP impacts on the oceanic ASM.

The vertical structure of the ASM also varies in response to the thermal effect of the TIP. As many studies have demonstrated (Schneider and Lindzen 1977; Schneider 1977, 1987; Held and Hou 1980), the atmospheric meridional circulation adopts two distinct regimes in response to axisymmetric diabatic heating, specifically the thermal equilibrium regime in the extra-tropics and the angular momentum conservation regime in the tropics. Under the regime of angular momentum conservation in the ASM region, a strong ascending motion is generated by the easterly vertical wind shear (Wu et al. 2015). In the tropics, the horizontal temperature advection is weak, and the diabatic heating is mainly balanced by the adiabatic ascent and cooling. Figure 3 presents the June–July–August (JJA) mean meridional circulation zonal averaged over the longitudinal range of 75–110°E in different experiments and the differences between them. As shown in Fig. 3a, the vertical velocity component shows strong ascending motion over the South Asian ocean region and the southern slope of the TIP in the CON run. The ridge line of the subtropical anticyclone is located above the southern slope of the TIP. When the sensible heating of the TIP is removed, the major ascending branch over the southern slope of the TIP disappears, and the South Asian High ridge line shifts southward to nearly 20°N in the TIPNS (Fig. 3b) in the troposphere. However, the vertical wind speeds over the Indian Ocean in the TIPNS run (Fig. 3b) are stronger than those in the CON run (Fig. 3a). Their difference (CON–TIPNS) demonstrates that the thermal effect of the TIP generates a monsoonal-type meridional circulation, with an ascending branch located over the southern slope of the TIP and a descending one over the tropical Indian Ocean (Fig. 3c). In summary, the ascending branch is responsible for the northern branch of the southern ASM.

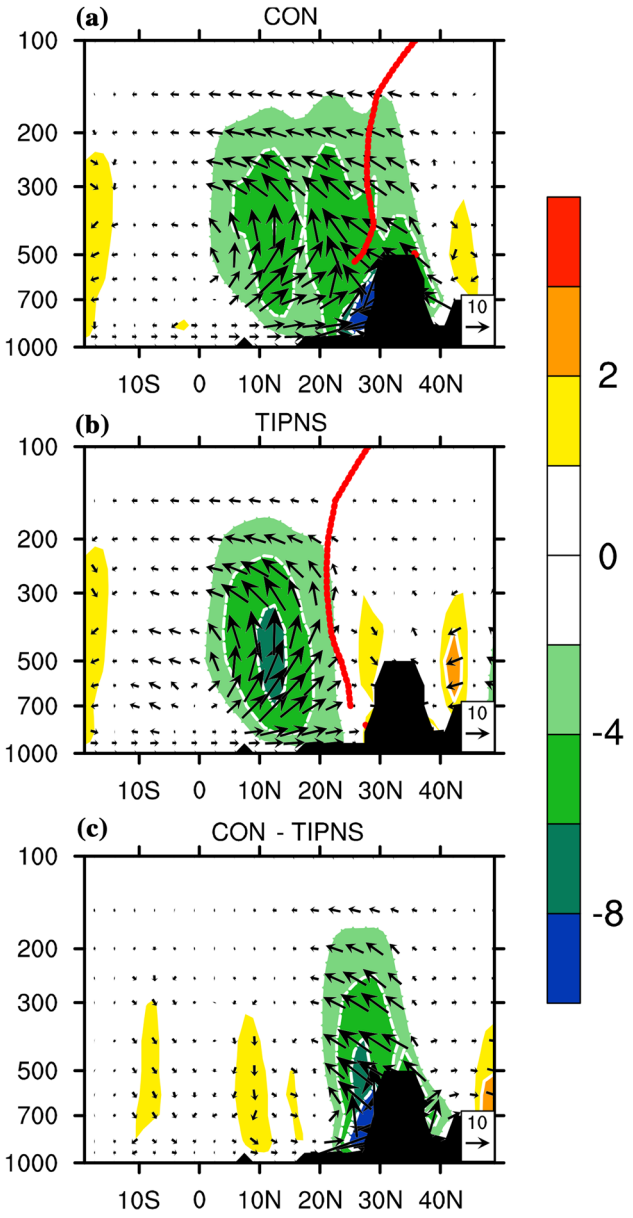

Fig. 3 Zonal averaged (75–110°E) June–July–August mean vertical velocity (shaded, 10^{-2} Pa s^{-1}) and the meridional circulation (vector, v in m s^{-1}, -3ω in 10^{-2} Pa s^{-1}) from the **a** CON, **b** TIPNS, and **c** CON–TIPNS experiments. The red line denotes the subtropical ridge line that satisfies $u = 0$ and $\partial u/\partial y > 0$. The black shading indicates the topography

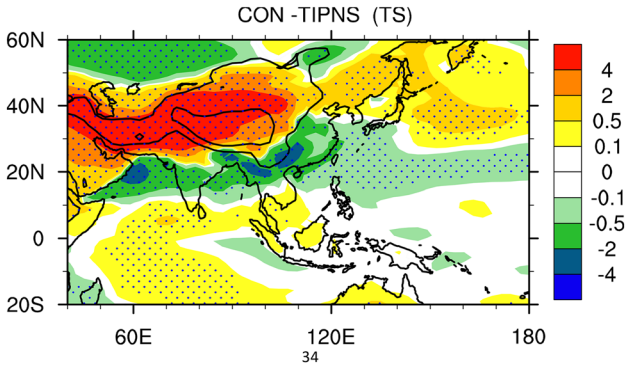

Fig. 4 June–July–August mean skin-surface temperature differences (K) between the CON and TIPNS experiments. The blue dots denote the values that pass a t-test with a significance level of 95%. The black contours indicate elevations of 1000 and 3000 m, respectively

4 Direct influence of the thermal effect of the TIP on the physical processes in the mixed layer of the Indian Ocean

4.1 Sea-surface temperature, mixed-layer temperature, and ocean current

As changes in SST are crucial to the surface diffusive heat flux and moisture flux from the ocean into the atmosphere, such temperature changes can significantly influence the ASM (Yeh et al. 1957; Duan and Wu 2005). We show the changes in the skin-surface temperatures over land and SST over ocean due to the thermal effect of the TIP in Fig. 4. The differences in skin-surface temperatures between the CON and TIPNS runs over the Asian continent show a decrease over the Indian subcontinent and central-eastern China, as well as an increase over the whole TIP region. In the ocean domain, the SST decreases over the AS, the BOB, the eastern equatorial Indian Ocean, and the subtropical western Pacific, and increases over the tropical Indian Ocean and the mid-latitudes of the northwestern Pacific. These decreases resemble those noted by Abe et al. (2013), who found that the SST decreased in the AS when the TP was removed in a CGCM and attributed these differences to the changes in heat flux driven by anomalous ocean currents.

In general, the depth of the mixed layer in the Indian Ocean is approximately 40–50 m during the boreal summer, where the mixed layer in the ocean is often defined as the layer between the sea surface and the lowest depth with a vertical temperature difference less than 0.5 °C (Montégut et al. 2004; Lin et al. 2011; He and Wu 2013). To obtain the three-dimensional features of ocean temperature and current, in Fig. 5 we show the spatial characteristics of the ocean temperature and current differences between the CON and TIPNS runs at depths of 5, 25, 45, and 85 m, representing the near surface, the middle of the mixed layer, the intersection between the mixed layer and the thermocline, and the thermocline, respectively.

The seawater at the depth of 5 m (Fig. 5a) cools within the northern AS, the northern BOB, and the western coast of Indonesia, and warms within most of the tropical Indian Ocean. This pattern is very similar to the changes in SST shown in Fig. 4, with both panels showing a low SST off Sumatra and a high SST in the western Indian Ocean, accompanied by 850-hPa wind and precipitation anomalies as shown in Fig. 2b,

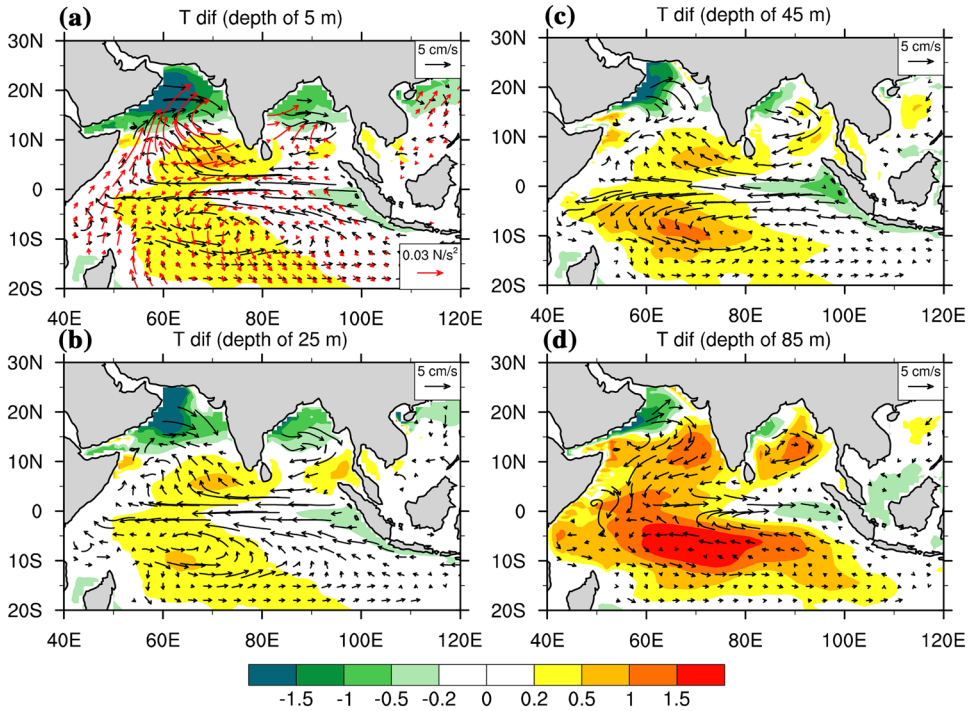

Fig. 5 June–July–August mean differences between the CON and TIPNS runs for the seawater temperatures (shaded, °C) and ocean currents (black vectors, cm s^{-1}) at the depths of **a** 5 m, **b** 25 m, **c** 45 m, and **d** 85 m. The red arrows in **a** denote the surface wind stress (10^{-2} N s^{-2})

which resemble the Indian Ocean Dipole pattern along the equator (Saji et al. 1999). Forced by changes in the surface wind stress (red vectors), water flows to the west along the equator (black vectors) and turns northward along the eastern coast of Africa and the Arabian Peninsula into the northern AS. At 25 m depth (Fig. 5b), in the middle of the mixed layer, the changes in temperatures and currents are similar to those at 5 m, except that the current in the northern AS is slightly weaker. At 45 m depth (Fig. 5c), close to the bottom of the mixed layer, the cooling of seawater within the AS is significantly weakened, whereas the cooling over the BOB almost disappears. At this depth, the western tropical Indian Ocean is warmer than at 5 m, and the cooling along the western coast of Indonesia is stronger. At greater depths below the thermocline, such as at 85 m (Fig. 5d), the seawater warms over the entire Indian Ocean. Moreover, the ocean currents flow from the northern AS to the tropics, which then turn eastward along the equator to the western coast of Indonesia, before reversing direction relative to those above the thermocline.

4.2 Surface radiation and heat fluxes

Changes in SST are strongly affected by the fluxes of radiation and heat at the sea surface. To understand the possible causes of the changes in SST, we first calculate the surface radiation budget in the Indian Ocean. The surface net radiation budget can be expressed as

$$F_{net}^{sfc} = F_{sw}^{D}\left(1 - A_{sfc}\right) + F_{lw}^{D} - F_{lw}^{U} \quad (4)$$

where F_{net}^{sfc} represents the surface net downward radiation; F_{sw}^{D} represents the surface downward shortwave radiation; A_{sfc} represents the surface albedo; and F_{lw}^{D} and F_{lw}^{U} represent the surface downward and upward longwave radiation, respectively. Changes in the skin-surface temperature are influenced by changes in downward radiation, which are in turn affected by changes in the cloud distribution. Therefore, we show the changes in the total cloud cover resulting from the thermal forcing of the TIP (CON–TIPNS) in Fig. 6a, which shows that the total cloud cover increases over the western tropical Indian Ocean and the South Asian continent, with a maximum centered over the southeastern slope of the TP. The cloud cover decreases prominently over central Asia and slightly over the Maritime Continent in the tropics. The pattern of change in total cloud cover results in a strong decrease in F_{sw}^{D} (Fig. 6b) over the South Asian continent, a weak decrease over the western Indian Ocean, and an increase over the Maritime Continent and the eastern tropical Indian Ocean. The net surface shortwave radiation $F_{sw}^{D}\left(1 - A_{sfc}\right)$ (Fig. 6c) shows a similar pattern toF_{sw}^{D}, indicating a relatively small impact of the change in surface albedo, with almost all the change in net downward solar energy resulting from the change in insolation. The surface downward longwave radiation F_{lw}^{D} increases primarily over the South Asian continent and the Indian Ocean (figure not shown) consistent with the cloud-cover distribution. Consequently, F_{net}^{sfc} decreases significantly over the AS, the BOB, the northwestern Pacific Ocean, and southern South Asia (Fig. 6d). Over the Indian Ocean, the distribution is similar

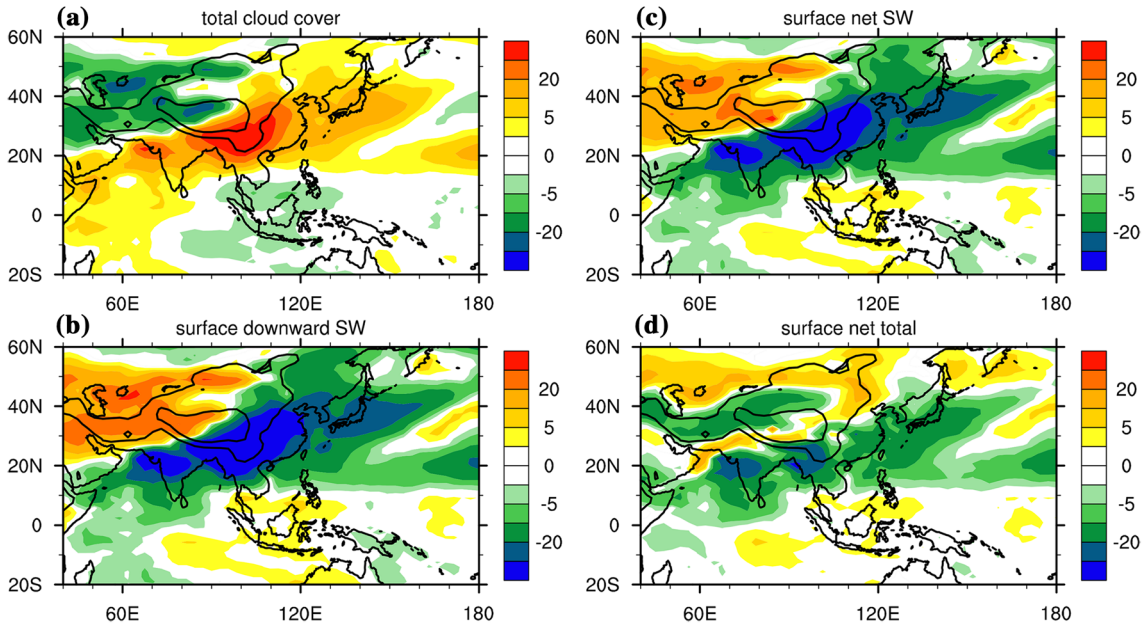

Fig. 6 June–July–August mean differences between the CON and TIPNS runs of **a** total cloud cover (%), **b** surface downward shortwave radiation (W m^{-2}), **c** surface downward net shortwave radiation (W m^{-2}), and **d** surface total net downward radiation (W m^{-2}). The black contours indicate elevations of 1000 and 3000 m, respectively

to the distribution of changes in downward shortwave radiation, F_{sw}^{D} (Fig. 6b). By comparing this distribution to the observed distribution of changes in SST (Fig. 4), we find that the warming in the southern Indian Ocean is quite consistent with the local increase in F_{net}^{sfc}, and the cooling over the AS, the BOB, and the monsoon region in the northern Indian Ocean is consistent with the local decrease in F_{net}^{sfc}. However, the SST warming in the central tropical Indian Ocean cannot be explained by the change in F_{net}^{sfc} alone. Further analysis is provided in the next section.

Figure 7 shows the influence of the thermal effect of the TIP on changes in the surface heat fluxes and the associated water–vapor transport (CON–TIPNS). The surface sensible heat flux (Fig. 7a) primarily increases over the whole TIP due to the experiment design, and decreases over the ASM region, which is connected to the increase in precipitation over this area (Fig. 2b). The surface sensible heat flux also decreases over the northern AS and the BOB in good agreement with the decrease in the SST change (Fig. 4). However, the changes in the surface sensible heat flux are quite weak over the whole Indian Ocean. The surface latent heat flux increases strongly over East Asia and the southeastern TP (Fig. 7b) in response to the thermal effect of the TIP. Over the ocean, the surface latent heat flux decreases over the northwestern Pacific, the central AS, and the tropical Indian Ocean, but increases over the western Indian Ocean. The surface latent heat flux decreases by more than 10 W m^{-2} in the eastern AS, and this change coincides with the maximum in situ SST warming, which exceeds 0.5 K (Figs. 4, 5a). The decrease in the surface latent heat flux in the area from the central AS to the north of the equator, which is connected with a decrease in evaporation (Fig. 7c), also contributes to the local SST increases, as shown in Fig. 4. This result implies that the thermal forcing of the TIP reduces the surface latent heat flux and contributes to the SST increase over the central and eastern tropical Indian Ocean through reducing the surface wind speed in this region (Fig. 5a). In correspondence with enhanced circulation at 850-hPa surrounding the TIP (Fig. 2b), the thermal effect of the TIP induces a large amount of water vapor to the south of the TIP and to the north of approximately 10°N, contributing to the remarkable increase in the vertically integrated water vapor over subtropical South and East Asia, whereas the vertically integrated water vapor decreases prominently over the area to the northwest of the TIP (Fig. 7d).

4.3 Energy budget in the mixed layer of the Indian Ocean

The changes in SST may also be attributed to changes in the physical processes occurring in the ocean mixed layer. Here, we analyze the causes of these SST changes in the mixed layer using the heat budget equation

$$\underset{\text{A}}{\frac{\partial T}{\partial t}} = \underset{\text{B}}{\frac{Q_{net} - Q_{pen}}{\rho_0 c_p H}} - u\underset{\text{C}}{\frac{\partial T}{\partial x}} - v\underset{\text{D}}{\frac{\partial T}{\partial y}} - w\underset{\text{E}}{\frac{\partial T}{\partial z}} + \varepsilon, \tag{5}$$

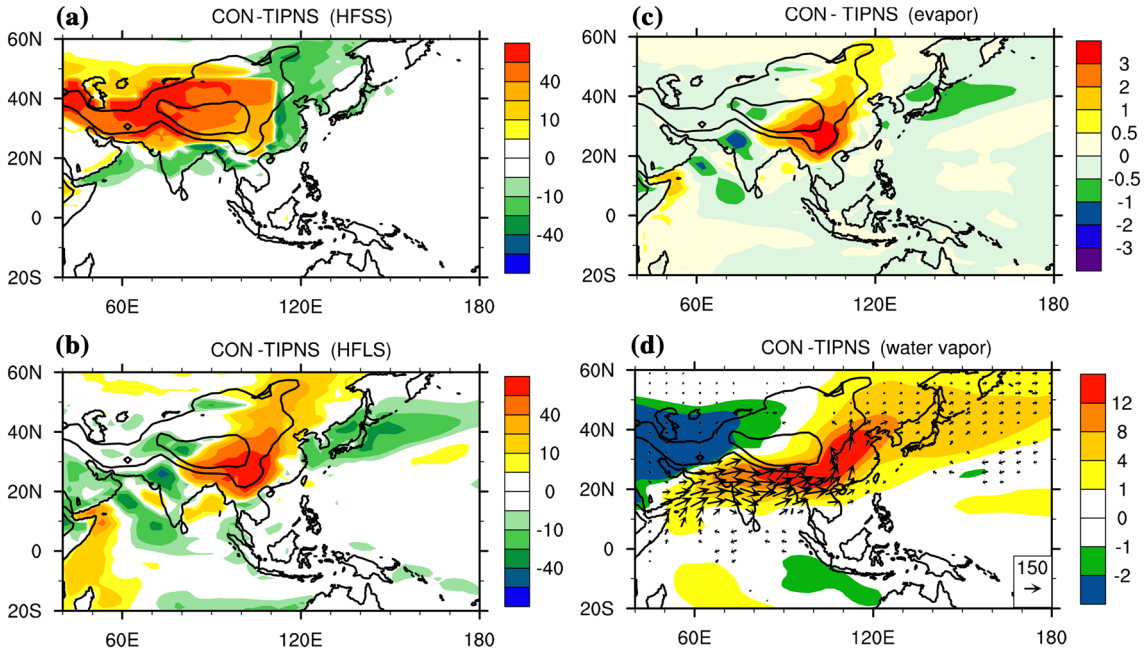

Fig. 7 June–July–August mean differences between the CON and TIPNS runs of **a** sensible heat fluxes (W m^{-2}), **b** latent heat fluxes (W m^{-2}), **c** surface evaporation (mm day^{-1}), and **d** vertically integrated water vapor (shaded, kg m^{-2}) and the 850-hPa water vapor fluxes (vector, kg m^{-1} s^{-1}). The black contours indicate elevations of 1000 and 3000 m, respectively

where T represents the temporally averaged mixed-layer temperature, $H = 45$ m represents the mixed-layer depth, Q_{net} represents the net surface heat flux, Q_{pen} represents the shortwave penetration through depth H, u represents the zonal current, v represents the meridional current, and w represents the current vertical velocity component. The vertical means of the oceanic terms are calculated as

$$\overline{()} = \frac{1}{H}\int_{-H}^{0} dz. \tag{6}$$

The seawater has a density (ρ_0) of 1.029×10^3 kg m^{-3} and a specific heat (c_p) of 3996 J kg^{-1} K^{-1}. The calculation of Q_{pen} follows the solar radiation penetration parameterization scheme introduced by Paulson and Simpson (1977) as

$$Q_{pen} = SW \times (R \times e^{-H/L_1} + (1-R)e^{-H/L_2}) \tag{7}$$

where SW is the downward shortwave radiation at the sea surface, $R = 0.58$, $L_1 = 0.35$ m and $L_2 = 23$ m. In Eq. (5), term A denotes the local temperature change; terms B to E are the net heat fluxes, the horizontal advection, and the vertical mixing, respectively; and the last term, ε, represents the sum of the horizontal and vertical diffusion of temperature, which is relatively small (Lin et al. 2007).

To further understand the temperature changes in the mixed layer of the Indian Ocean, we calculate each term of the budget in Eq. (5) and analyze their relative contributions to the temperature changes within this layer. Figure 8 shows the differences between the CON and TIPNS runs for each term in Eq. (5). The difference for term A (Fig. 8a), which is the difference of the local change in vertical mean ocean temperature in the mixed layer, shows a similar distribution to that of the mean changes in SST (Fig. 4), with significant cooling within the northern AS, the BOB, and off the western coast of Indonesia, and warming within the middle tropical Indian Ocean. The sum of the B, C, D, and E terms on the right-hand side of Eq. (5) is shown in Fig. 8g, indicating a similar pattern to that of the vertically integrated mixed-layer temperature change (Fig. 8a), implying the calculations on both sides of Eq. (5) are generally balanced.

Term B is related to the surface net heat flux, which decreases by 0.1–0.5 °C $month^{-1}$ in the western Indian Ocean, the northeastern AS, and the northern BOB, but increases primarily over the northwestern AS (Fig. 8b). Importantly, the pattern of change in the heat fluxes is consistent with the changes in the surface latent heat flux (Fig. 7b) but with opposite signs, indicating the importance of ocean surface evaporation in the surface energy budget in these areas. Within the tropical Indian Ocean, the differences in term B over the western Indian Ocean have an opposite sign to that over the central and eastern Indian Ocean. The zonal advection term C (Fig. 8c) generates cooling in the northern AS and warming over the western Indian Ocean, but also a weak cooling within the BOB and off the western coast of Indonesia. The meridional advection term D (Fig. 8d) also shows a strong cooling

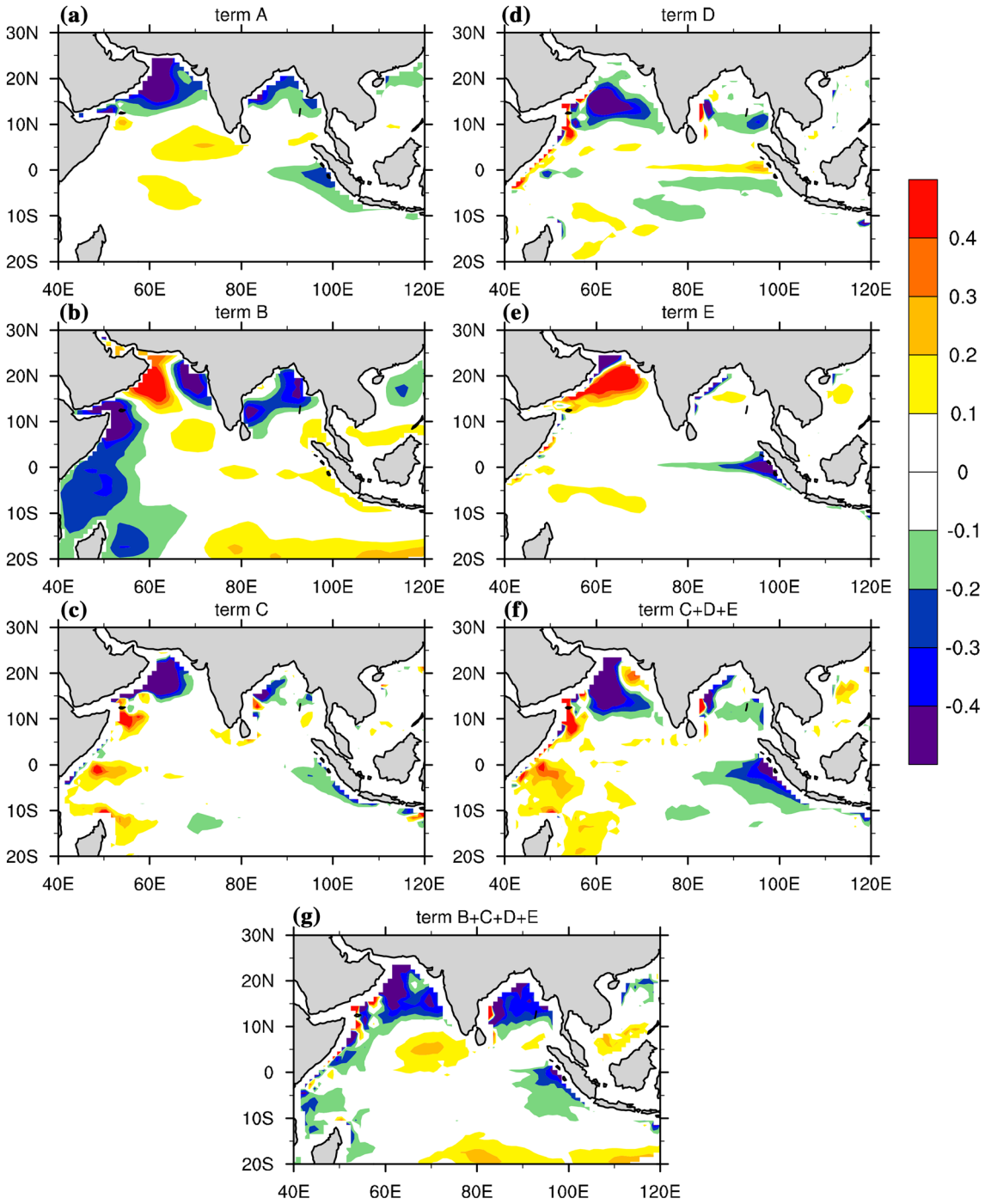

Fig. 8 June–July–August mean differences between the CON and TIPNS runs of the mixed layer (0–45 m) heat budget (°C month^{-1}) calculated using Eq. (5) for the terms **a** A, **b** B, **c** C, **d** D, and **e** E; **f** the sum of terms C, D, and E; and **g** the sum of terms B, C, D, and E

over the AS, a weak cooling over the BOB and along 10°S in the Southern Hemisphere, and a weak warming near 5°N in the Northern Hemisphere. The vertical mixing term E (Fig. 8e) shows prominent warming in the northern AS and in the Seychelles, implying strong downwelling in these ocean regions. This term also shows strong cooling along the western coast of Indonesia extending to the equator, which implies strong upwelling in the mixed layer. To compare the contributions of changes in heat flux and advection, terms C, D, and E are summed, with the results presented in Fig. 8f, showing that the warming over the western Indian Ocean resulting from advection is mostly counteracted by the cooling from the heat

flux (Fig. 8b). Moreover, the cooling within the northern AS, the BOB, and off the western coast of Indonesia, is similar to the changes in term A, showing the importance of horizontal advection and upwelling/downwelling in determining the temperature change in these regions. However, the cooling in the northern AS and the BOB as shown in Fig. 8b is closely connected to the changes in the radiation flux (Fig. 6d).

Based on the above analysis of the changes in the temperature, circulation, and heat budget of the mixed layer in the South Asian oceans, the major effects of the thermal forcing of the TIP on the changes in subsurface temperatures and ocean dynamics can be summarized as follows. The thermal forcing of the TIP enhances the westerlies over the northern AS and the BOB (Fig. 2b) in the lower troposphere, thereby intensifying the near sea-surface wind stress (Fig. 5a). The decrease in the net surface heat flux, together with the horizontal advection, contributes to the cooling of the mixed layer within the northern AS and the BOB. The cooling off the western coast of Indonesia is mainly caused by local upwelling. The warming within the tropical Indian Ocean is a consequence of the contributions from multiple causes, including the increased heat fluxes, horizontal advection, and downwelling. An exchange of seawater between the mixed layer and the thermocline is also observed. The seawater in the mixed layer flows from the tropics into the northern AS, where the seawater sinks into the deep ocean (Fig. 8e).

The results shown in Figs. 5 and 8e, f clearly demonstrate that the thermal forcing exerted by the TIP can generate remarkable westward tropical ocean currents in the mixed layer of the Indian Ocean (Fig. 5a–c). These currents sink and penetrate the thermocline into the deep ocean in the western tropical Indian Ocean, then flow eastward towards the eastern Indian Ocean in the thermocline (Fig. 5d). Finally, these ocean currents ascend in the eastern tropical Indian Ocean, bringing cold water from the deep ocean upward, penetrating the thermocline, and reaching the near-surface layers (Fig. 8e). These processes produce a trans-thermocline longitudinal circulation in the tropical Indian Ocean that includes downwelling currents in the west and upwelling currents in the east. An SST anomaly pattern similar to an Indian Ocean Dipole is therefore produced, with a reduced SST located off the western coast of Indonesia, and an increased SST located in the western Indian Ocean.

5 Indirect influence of the thermal effect of the TIP on the Asian summer monsoon

5.1 Indirect effects on precipitation and circulation

As defined in Sect. 2, the indirect effect of TIP thermal forcing can be expressed as Eq. (1) or (2). For the right-hand side of these two equations, the first term (CON–TIPNS) was presented in Fig. 2b, and the last terms (CON_CPSST–TIPNS_CPSST) and (CON_NSSST–TIPNS_NSSST) can be found in Fig. S2a, and S2b in OSM. Comparison of the differences of the monsoonal precipitation between the coupled (Fig. 2b) and uncoupled (Fig. S2a and b in OSM) runs shows that the largest differences occur over the Indian Ocean, which indicates the important role of the indirect effect in regulating the thermal impacts of the TIP on the ASM. For the DD_CPSST case, the precipitation anomaly (Fig. 9a) mainly decreases over the southern slope of the TP, the western AS, and the tropical Indian Ocean, and is accompanied by an anomalous anticyclonic circulation around the TIP at the 850-hPa level. Meanwhile, the precipitation difference increases mainly in the northeastern AS, south Iranian Plateau, most parts of the BOB, and the Indian mainland, which is accompanied by anomalous westerly surface winds over the AS. In general, the distribution pattern of the differences in rainfall shown in Fig. 9a is the opposite pattern to the rainfall differences between the CON_CPSST and TIPNS_CPSST runs shown in Fig. S2a in OSM. This result suggests that the indirect effect on the ASM tends to counteract the TIP–SHAP direct forcing, which reduces the amount of precipitation falling over the southern Himalayas but intensifies rainfall from the northeastern AS to the western Pacific.

The changes in precipitation are closely related to the changes in the meridional circulation in ASM region. The vertical circulation of DD_CPSST is shown in Fig. 9c. The figure indicates that a strong ascent of air over the Indian mainland (10–20°N), accompanied by a strong descent over south slope of the TP. The above features correspond to the in situ difference in surface easterly winds and reduced precipitation (Fig. 9a). These results indicate that the indirect effect of the thermal forcing of the TIP resulting from the air–sea interactions tends to counteract its direct effect by enhancing the monsoonal meridional circulation around 10–20°N and generating an anti-monsoonal meridional circulation further north.

For the DD_NSSST case, the difference patterns of precipitation and circulation shown in Fig. 9b and meridional circulation shown in Fig. 9d are similar to their counterparts in the DD_CPSST case as shown in Fig. 9a, c, respectively. These results imply that the indirect impacts demonstrated in Fig. 9 are well preserved and not very sensitive to the imposed SST. Figure 10 shows the indirect effect on the skin-surface temperature. Because the SST difference between the CON_CPSST and TIPNS_CPSST runs, or between the CON_NSSST and TIPNS_NSSST runs, is zero, the indirect impact on the skin-surface temperature over oceans is exactly equal to the CON–TIPNS result (Fig. 4). The temperature difference mainly appears as a positive–negative–positive pattern in the meridional

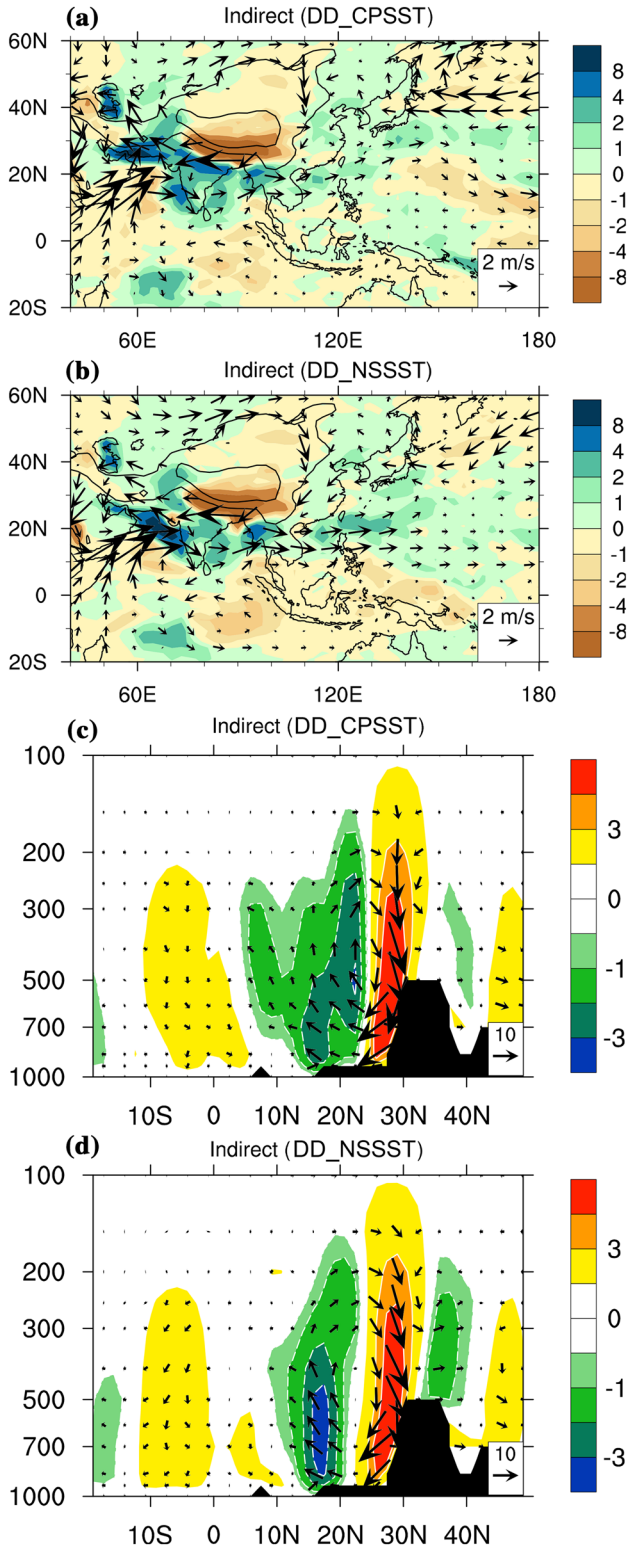

Fig. 9 Indirect effect of the TIP thermal forcing on the JJA mean ASM generated from **a, c** [(CON − TIPNS)−(CON_CPSST − TIPNS_CPSST)] and **b, d** [(CON − TIPNS)−(CON_NSSST − TIPNS_NSSST)]. **a, b** Precipitation (shading, mm day^{-1}) and 850-hPa wind speed (vectors, m s^{-1}); and **c, d** the 75–110°E mean vertical velocity component (shaded, 10^{-2} Pa s^{-1}) and meridional circulation (vectors, v in m s^{-1}, -3ω in 10^{-2} Pa s^{-1}). The black contours indicate elevations of 1000 and 3000 m, respectively. The black shading in **c, d** indicates the topography

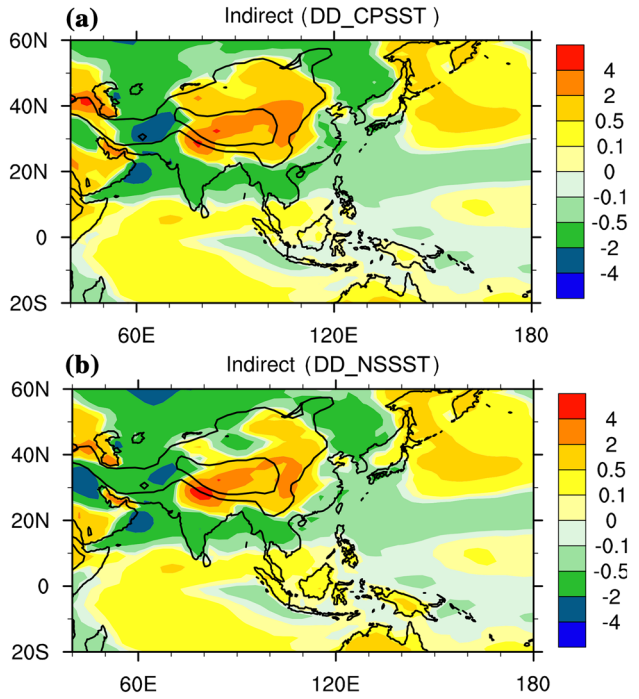

Fig. 10 Indirect effect of the TIP thermal forcing on the JJA mean skin-surface temperature (K) generated from **a** [(CON − TIPNS)−(CON_CPSST − TIPNS_CPSST)] and **b** [(CON − TIPNS)−(CON_NSSST − TIPNS_NSSST)]. The black contours indicate elevations of 1000 and 3000 m, respectively

direction over the 70–120°E section. Corresponding to this sandwich-like pattern of skin-surface temperature difference, strong anomalous westerly winds occur at the 850-hPa level along 15°N, and easterlies are produced near the equator (Fig. 9a, b). In combination with the anticyclonic circulation surrounding the TIP, a prominent surface circulation dipole develops to include a cyclone to the north of 15°N and an anticyclone to its south. This circulation dipole is accompanied by higher precipitation along the zonal belt between 10°N and 15°N and lower precipitation to its south and north. This rainfall pattern accompanies a stronger air ascent along 10–20°N and air descent over the southern slope of the TIP and over the southern tropics (Fig. 9c, d). Thus, the presence of air–sea coupling in the CGCM increases the strength of the southern branch of the South Asian summer monsoon compared with that for the AGCM, whereas its northern branch is weakened. Thus, the similar responses to the TIP indirect forcing of the precipitation, skin-surface temperature, and circulation between the DD_NSST and DD_CPSST (Figs. 9, 10) confirms the indirect effect of TIP thermal forcing is not sensitive to the different SST, which was adopted from CGCM experiments.

5.2 Hydrological cycle and surface fluxes related to the indirect effects

We present here the responses of the hydrological cycle, the surface net heat fluxes, and the radiation budget to the TIP indirect forcing as demonstrated in the DD_CPSST. In terms of the hydrological cycle, the indirect effects of the TIP heating on the changes in water–vapor transport and evaporation are shown in Fig. 11a, e, respectively. The transport of water vapor decreases over TP in association with the anticyclone anomaly, which contributes to the decrease in precipitation. The water vapor increases mainly from Indian mainland, and northern BOB to East Asia, associated with the intensified westerlies. The changes of the evaporation anomaly (Fig. 11e) are weak compared with the changes in water vapor in the atmosphere (Fig. 11a). Therefore, the increase of precipitation in DD_CPSST is mainly attributed to the increase of water vapor over Asian mainland. However, in the northern Indian Ocean, the decreased SST over the northern AS (Fig. 10a) leads to local decreases in evaporation (Fig. 11e), which is the main cause of the decrease in precipitation over the western AS (Fig. 9a). For sensible heat flux (Fig. 11b), there is typically a positive anomaly over the TP and negative anomaly over the Indian mainland and the Indo-China peninsula, which is closely connected to the changes in the precipitation and radiation budget.

In terms of changes in surface radiation budgets, the cloud cover (Fig. 11c) increases over South Asia and northern AS but decreases over the TP, which leads to the increased F_{sw}^{D} in southern edge of the TP and the decreased F_{sw}^{D} in the Iranian Plateau, northern AS, and south Asian sub-continent (Fig. 11g). The responses of F_{lw}^{D} are weak over the Indian Ocean, but an increase of more than 5 W m^{-2} occurs over the Indian mainland and East Asia (Fig. 11d). The spatial pattern of F_{net}^{sfc} (Fig. 11h) is similar to that of F_{sw}^{D} (Fig. 11g), indicating the dominant role of cloud cover and shortwave radiation in the radiation changes induced by the indirect effect. The radiation effect leads to a reduced SST in the northern AS and BOB, and an increased SST mainly in the western and tropical Indian Ocean.

In short, the indirect thermal effect of the TIP suggests that oceanic feedbacks to the atmosphere have an important role. Specifically, these feedbacks generate sandwich-type SST and circulation anomaly over Indian Ocean and south Asian continent, associated with cloud, radiation, and water vapor changes. Together, these processes reflect a complete physical representation of the response of the ASM to the indirect thermal effect of the TIP through changes in the local hydrological processes, which counteracts the direct thermal effect of the TIP on the ASM and reduces its strength.

6 Uncertainties in evaluating the indirect effects

Because of model bias, the SST generated from the CGCM (i.e., CPSST) is different from the observed SST. Thus, the indirect effects obtained from the DD_CPSST run may be also different from those obtained from the experiments based on the observed SST. To improve our understanding of the TIP thermal effects on ASM, it is important to analyze the influence of the SST bias, and to assess the uncertainty of the indirect effects of the TIP thermal forcing.

6.1 Impacts of the sea-surface temperature bias

Figure 12a shows the bias of the SST generated from the CGCM. The bias is calculated from the difference of the mean SST during JJA between the coupled control experiment (CON) and the observed SST, which is used to drive the AGCM experiment (CON_OBSST). In the Indian Ocean, the cold bias occurs over the AS, the BOB, and off the western coast of Sumatra, while the warm bias occurs in the tropical and southern Indian Ocean. In the western Pacific, the warm bias mainly occurs in mid-high latitudes and along the equator, while the cold bias appears in both the northern and southern tropics. Notice that the influence of SST bias on the control and sensitivity runs can be expressed as

$$\mathrm{D\_SH} = \mathrm{CON} - \mathrm{CON\_OBSST}, \tag{8}$$

$$\mathrm{D\_NS} = \mathrm{TIPNS} - \mathrm{TIPNS\_OBSST}. \tag{9}$$

For D_SH = (CON − CON_OBSST), in both the CGCM experiment CON and the AGCM experiment CON_OBSST, the surface sensible heating exists over the TIP, where the difference inherent in D_SH exhibits the main impacts of the SST bias (Fig. 12a). Similarly, for D_NS = (TIPNS − TIPNS_OBSST), in both the CGCM experiment TIPNS and the AGCM experiment TIPNS_OBSST, the surface sensible heating over the TIP is excluded, and the difference contained in the D_NS run also exhibits the main impacts of the SST bias (Fig. 12c).

The distributions of JJA mean precipitation and the wind speed at 850-hPa calculated from the D_SH and D_NS runs are presented in Fig. 12b, d, respectively. Interestingly, the distributions of the difference in wind speed and precipitation are similar. In particular, the distribution of the difference in the precipitation over the ocean resembles that of the SST bias, respectively (Fig. 12a, c), where a positive (negative) precipitation difference appears where the SST bias is positive (negative). The differences in the SST bias are mainly located over the AS and BOB, where D_NS (Fig. 12c) shows weaker SST negative bias over the south

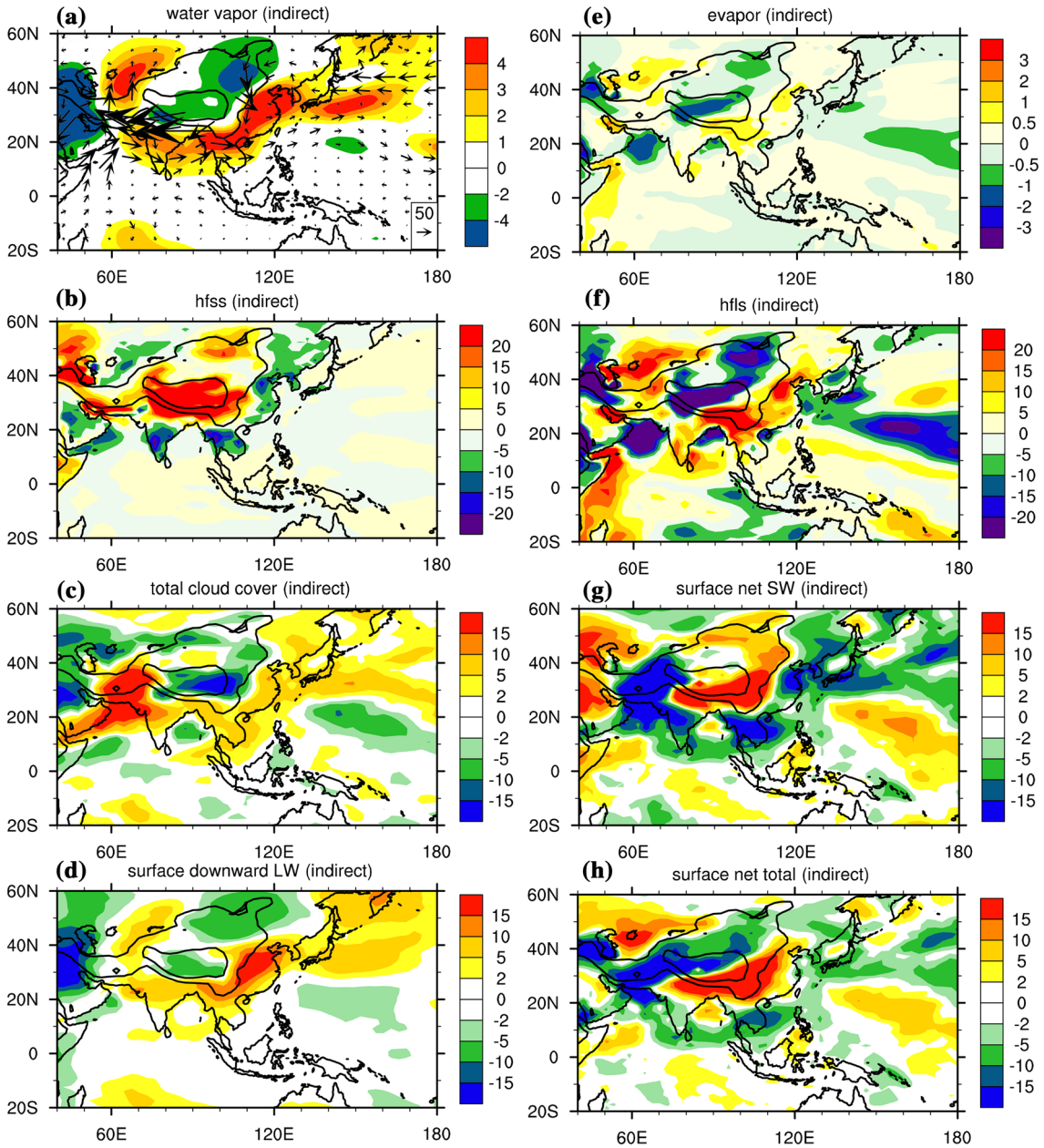

Fig. 11 Indirect effect of the thermal forcing associated with the TIP on the JJA mean ASM [(CON − TIPNS)−(CON_CPSST − TIPNS_CPSST)]. **a** Vertically integrated water vapor (shaded, kg m^{-2}) and 850-hPa water vapor fluxes (vectors, kg m^{-1} s^{-1}), **b** surface sensible heat fluxes (W m^{-2}), **c** total cloud cover, **d** surface downward longwave radiation fluxes (W m^{-2}), **e** surface evaporation (mm day^{-1}), **f** surface latent heat fluxes (W m^{-2}), **g** surface net shortwave radiation fluxes (W m^{-2}), and **h** surface net radiation fluxes (W m^{-2}). The black contours indicate elevations of 1000 and 3000 m, respectively

AS and BOB but positive SST bias over the north AS. Weak precipitation occurs over northern Indian Ocean and extremely strong precipitation over the south slope of TP in the CON_CPSST and CON_NSSST because of the SST bias, as shown in Fig. S1b and c in the OSM. These results demonstrate that the SST bias is an important issue that should be considered when conducting numerical experiments. The uncertainties are identified in the following sub-section.

6.2 Uncertainty of the indirect effects

To further evaluate the degree of the impacts of SST bias on the simulation, and the uncertainty of the indirect effects of the TIP thermal forcing, we estimate the indirect effects

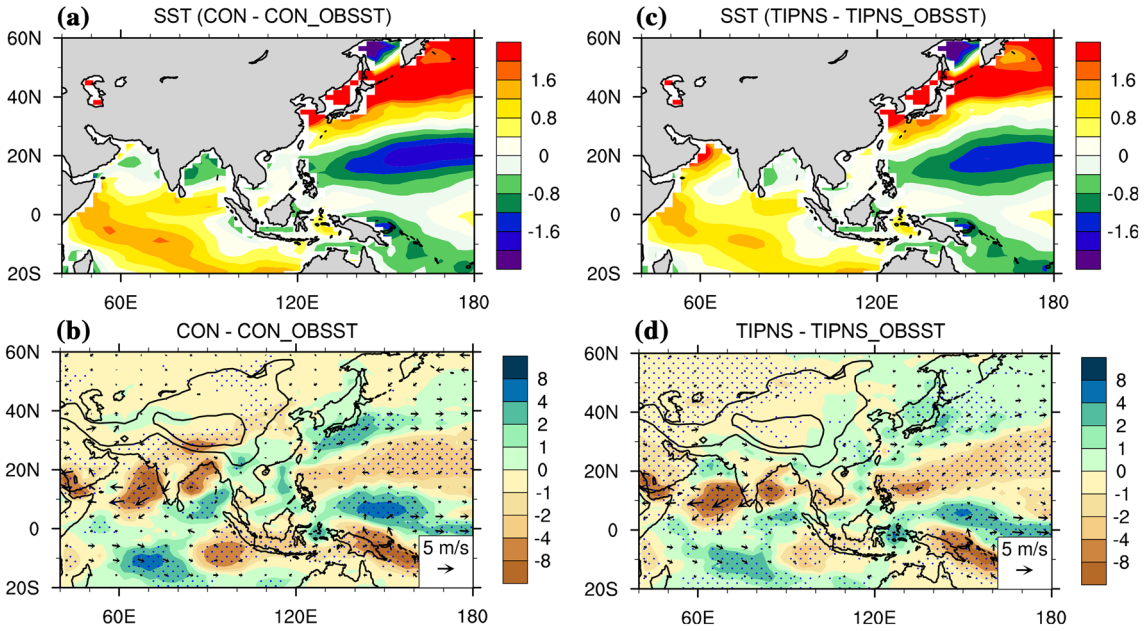

Fig. 12 June–July–August mean difference of **a** mean SST (K) between the CON and CON_OBSST runs, and **c** the TIPNS and TIPNS_OBSST, and of precipitation (shaded, mm day^{-1}) and 850-hPa wind speed (vectors, m s^{-1}) between (**b**) the CON and CON_OBSST runs, and **d** the TIPNS and TIPNS_OBSST runs. The blue dots in **b, c** denote the precipitation difference passing the 95% significance *t*-test, and the black contours denote elevations of 1000 and 3000 m, respectively

of TIP following the approach used by Kitoh (2004) and Okajima and Xie (2007), who defined the indirect effect of the TIP thermal forcing (DD_OBS) as shown in Eq. (3) using the observed SST-driven AGCM. Since Eq. (3) can be rewritten as

$$\begin{aligned} \text{DD\_OBS} &= (\text{CON} - \text{CON\_OBSST}) \\ &\quad - (\text{TIPNS} - \text{TIPNS\_OBSST}), \end{aligned} \tag{10}$$

and since the first and second terms on the right-hand side of Eq. (10) possess similar distributions (Fig. 12b, d) and suffered from similar SST biases (Fig. 12a, c), the experiment design in Eq. (3) could mitigate the impacts of the SST bias to some extent.

The distributions of the precipitation, wind speed at 850-hPa, skin-surface temperature, and meridional circulations produced from the DD_OBS are presented in Fig. 13. In comparison with Figs. 9 and 10, the indirect effects obtained from these three sets of experiments (DD_OBS, DD_CPSST, and DD_NSSST) possess the following common features:

(a) Near the surface, a remarkable anticyclone circulation surrounds the TIP; to its south is a cyclonic circulation located over the northern Indian Ocean and another anticyclone circulation located further south over the tropical Indian Ocean, exhibiting a triple horizontal circulation pattern. An intensified tropical westerly flow is located over the northern Indian Ocean between the cyclone circulation in the north, and the anticyclone circulation in the south (Fig. 9a, b, 13a).

(b) The precipitation triple pattern in Fig. 9a, b is also reproduced over the South Asian summer monsoon area in this experiment, with increased precipitation appearing along with the intensified tropical westerly flow, and reduced precipitation over the southern slope of the TIP to the north, and over the tropical Indian Ocean to the south.

(c) A dipole meridional circulation develops over the Indian Ocean, with the ascending arm located over the tropical Indian Ocean in coordination with the increased precipitation and two descending arms located over the southern slope of the TIP and the southern tropical Indian Ocean (Fig. 9c, d, 13c).

Results from the above analysis imply that indirect effects on the ASM of the TIP thermal forcing presented in Sect. 5 have captured certain basic features in the changes of circulation and precipitation. Compared with the DD_OBS run, however, several noticeable differences can be identified from the DD_CPSST and DD_NSSST runs:

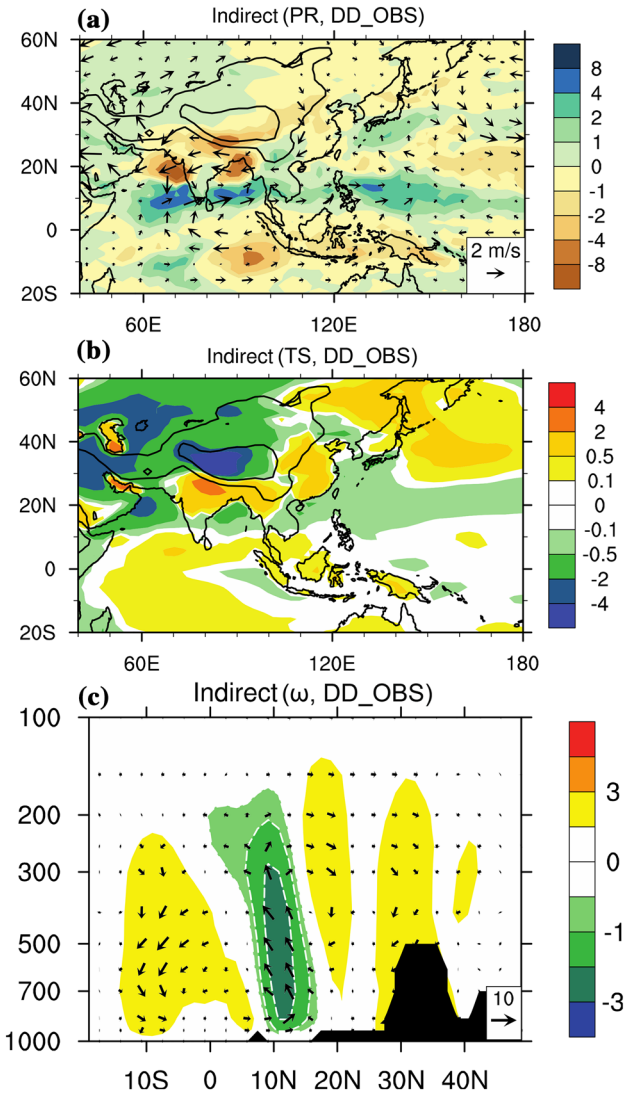

Fig. 13 Indirect effect (DD_OBS) of the thermal forcing associated with the TIP on the JJA mean ASM [(CON − TIPNS) − (CON_OBSST − TIPNS_OBSST)]. **a** Precipitation (shaded, mm day^{-1}) and 850-hPa wind speed (vectors, m s^{-1}); **b** surface temperatures (shaded, K); and **c** the 75–110°E mean vertical velocity (shaded, 10^{-2} Pa s^{-1}) and meridional circulation (vector, v in m s^{-1}, -3ω in 10^{-2} Pa s^{-1}). The black contours indicate elevations of 1000 and 3000 m, respectively. The black shading in **c** indicates the topography

(a) The cyclonic circulation over the northern Indian Ocean of the "triple horizontal circulation pattern" shrinks and shifts northward, and, accordingly, the intensified westerly flow shifts northward. At the same time, the anticyclone circulation in the tropical Indian Ocean extends westward, contributing to the enhanced southwesterly winds over the northwestern AS.

(b) The ascending arm of the "dipole meridional circulation" over the tropical Indian Ocean also shifts northward and is almost three times stronger in DD_CPSST than in DD_OBS.

(c) Consequently, remarkable precipitation differences between the DD_OBS experiment and the DD_CPSST and DD_NSSST experiments occur over the northern AS and the BOB: the precipitation decreases over these regions in the DD_OBS run (Fig. 13a) but increases in the DD_CPSST and DD_NSSST runs (Fig. 9a, b), demonstrating the largest uncertainty in the evaluation.

At present, it is difficult to explore what causes this uncertainty since biases may excite further feedbacks in the model simulations. However, the existence of these differences reminds us that there is some uncertainty when the CGCMs and AGCMs are employed to study the indirect impact of the TIP thermal forcing, and thus caution is required. For example, the differences of precipitation and circulation between CON_CPSST and CON_OBSST (Fig. S3 in OSM) suggest that SST bias could cause excessive precipitation on the south slope of the TP and reduced precipitation over the AS and BOB, accompanied by enhanced westerly flow over the south TP and easterly flow over the Indian Ocean. This result suggests that the indirect effect revealed by DD_CPSST is overestimated over the south slope of the TP and underestimated over the Indian Ocean.

7 Discussion and conclusion

Based on a series of experiments using a CGCM and one of its components, an AGCM, the thermal effects of the TIP on the changes in the ASM during the boreal summer were investigated. The influences of the direct TIP thermal forcing and indirect forcing induced by the air–sea interaction on the changes in monsoonal precipitation, circulation, and SST were analyzed.

The direct thermal effects of large-scale elevated topography TIP cause the precipitation to increase over the southern slope of the TP and East Asia, whereas the precipitation decreases over the northwestern Indian subcontinent. This behavior is also accompanied by cyclonic circulation around the TIP in the lower troposphere in both the AGCMs and CGCMs. The thermal forcing of the TIP also exerts a direct effect on the thermal status and circulation over the Indian Ocean. The changes in the SST and the temperatures of the mixed layer in the Indian Ocean are mainly caused by changes in atmospheric radiative forcing, surface latent heat fluxes, and the associated ocean dynamics. Meanwhile, the increased shortwave radiation over the southern Indian Ocean contributes to the increased SST. The cooling of the mixed layer within the northern AS and the BOB is mainly induced by decreases in the surface heat flux and horizontal advection, whereas the cooling over western Indonesia is mainly caused by local upwelling.

Finally, the major roles of the indirect effect of the TIP thermal forcing in affecting the ASM are summarized in the schematic diagram shown in Fig. 14.

(1) The surface heating of the TIP drives cyclonic circulation in the lower troposphere around the mountains (a) and transports a large amount of water vapor towards the TP, shifting the main rain belt into the Asian inland region. In contrast, precipitation is reduced over almost the entire Indian Ocean in the Northern Hemisphere.

(2) In response to the TIP thermal forcing, the SST in the tropical Indian Ocean is warmer in the case with the TIP surface heating, and a difference in zonal ocean circulation along the equator is produced between the mixed layer and the deep ocean through the thermocline, as shown by the blue arrows in (c). The downwelling in the western Indian Ocean takes heat from the near surface to the deep ocean, and increases the ocean temperatures, whereas the upwelling in the eastern Indian Ocean leads to a reduced SST off the western coast of Indonesia.

(3) The heating of the TIP-induced air–sea interactions over the Indian Ocean as indicated by the dashed double-sided arrow between (b) and (c) generates non-uniform spatial SST anomalies (Figs. 10, 13b). The atmosphere influences the ocean mainly through radiation (downward-pointing red arrow) and the surface wind stress. In contrast, the sea surface feeds back into the atmosphere (upward-pointing purple arrow) mainly through changes in surface latent heat fluxes and evaporation. Thus, the ocean triggers upward vertical motion over the tropical Indian Ocean (upward-pointing heavy red arrow between (a) and (b)) and the associated descent air over the southern tropical Indian Ocean and the southern slope of the TP regions (downward-pointing heavy red arrow between (a) and (b)), forming a meridional circulation dipole over the tropical Indian Ocean.

(4) For the indirect effect (b) near the surface, the northern meridional circulation corresponds to the difference in easterly flow located to the south of the TP, whereas the cross-equator southern meridional circulation corresponds to the easterly flow anomaly in the southern tropics and westerly flow anomaly in the northern tropics where the meridional gradient of the SST is large. Consequently, a tripole horizontal difference circulation pattern composed of anticyclonic–cyclonic–anticyclonic (A–C–A) motion is formed over the TIP and the Indian Ocean (fine red curves in (b)). Therefore, we conclude that the indirect effect of the TIP thermal forcing plays the role of counteracting its direct effect on the ASM.

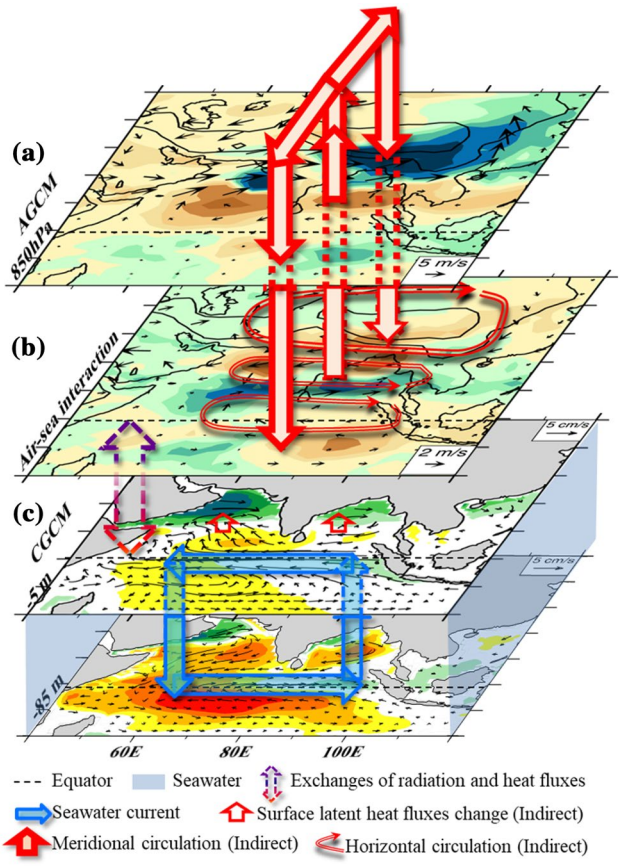

Fig. 14 Schematic diagram presenting the thermal effect of the TIP on the ASM. The direct effect of the TIP thermal forcing generates a cyclonic circulation in the lower troposphere around the TIP, while the indirect effect of the TIP thermal forcing generates an anticyclonic flow surrounding the TIP, and a cyclone–anticyclone circulation dipole to its south in the lower troposphere (fine red arrows), coupled with a pair of meridional circulations (bold red arrows), counteracting the TIP direct impact on the ASM. See text for details

It is important to note that comparison of the model outputs from CGCM and AGCM to study the indirect effects of the TIP thermal forcing on the ASM involves uncertainty. The SST generated in the CGCM is usually different from the observed SST employed to drive the AGCM. Thus, the difference in model output between the experimental pairs of the CGCM and the corresponding experimental pairs of the AGCM not only indicates the indirect effect of the TIP thermal forcing, but also involves some unwanted noise signals induced by the bias of the SST of the CGCM simulated from the observed SST. Sorting out the noise signals helps reduce the uncertainty in determining the indirect effect of the TIP forcing. Improving the CGCM performance and using multi-model ensemble can reduce the model bias as well as the noise signal, so as to mitigate the uncertainty.

We have investigated the influence of the surface sensible heating of the TIP on the climate mean ASM in the CGCM and compared it with that of the AGCM to reveal its indirect

effect on the ASM. However, we did not address how this indirect effect associated with the TIP thermal forcing affects the ASM variability. It is interesting to note that, along the equator, the SST response to TIP heating resembles the pattern of the Indian Ocean Dipole. Whether or not they have connections on an interannual scale needs further investigation. Moreover, the ASM and the associated SST variation also have close relations with the activities of the El Niño and the Southern Oscillation (Kawamura 1998). It is also unclear whether the thermal effect of the TIP is also influenced by these climate system factors, or by other physical processes, such as a reduction in cloud cover, responsible for the increase in the incoming solar radiation, leading to an enhancement in the heating of the TIP. Further studies on the interactions between the thermal effect of the TIP and SST variability and their relative contributions to the variability of the ASM will help in further understanding the dynamics of the ASM and in improving climate predictions.

Acknowledgements We would like to thank the two anonymous reviewers for their constructive suggestions that helped to improve the overall quality of the manuscript. This study was jointly funded by the National Natural Science Foundation of China (Grants 91637312, 91737306, 91437219, 91637208, 41730963, 41605038, and 41530426), the SOA Program on Global Change and Air–Sea Interactions (GASI–IPOVAI–03), the Open Projects of the Key Laboratory of Meteorological Disaster of Ministry of Education (grant no. KLME1405), and the Special Program for Applied Research on Super Computation of the NSFC–Guangdong Joint Fund (the second phase) under Grant No. U1501501. We thank Richard Foreman, PhD, and Alex Boon, PhD, from Liwen Bianji, Edanz Editing China (http://www.liwenbianji.cn/ac), for editing the English text of a draft of this manuscript.

References

Abe M, Kitoh A, Yasunari T (2003) An evolution of the Asian summer monsoon associated with mountain uplift—simulation with the MRI atmosphere–ocean coupled GCM. J Meteorol Soc Jpn Ser II 81(5):909–933

Abe M, Hori M, Yasunari T, Kitoh A (2013) Effects of the Tibetan Plateau on the onset of the summer monsoon in South Asia: the role of the air–sea interaction. J Geophys Res Atmos 118:1760–1776. https://doi.org/10.1002/jgrd.50210

Adler RF, Huffman GJ, Chang A et al (2003) The Version-2 Global Precipitation Climatology Project (GPCP) monthly precipitation analysis (1979–present). J Hydrometeorol 4:1147–1167

Bao Q, Wu GX, Liu YM et al (2010) An introduction to the coupled model FGOALS1.1-s and its performance in East Asia. Adv Atmos Sci 27: 1131–1142. https://doi.org/10.1007/s00376-010-9177-1

Bao Q, Lin PF, Zhou TJ et al (2013) The flexible global ocean–atmosphere–land system model, Spectral Version 2: FGOALS–s2. Adv Atmos Sci 30:561–576

Bolin B (1950) On the influence of the earth's orography on the general character of the westerlies. Tellus 2:184–195

Boos WR, Kuang ZM (2010) Dominant control of the South Asian monsoon by orographic insulation versus plateau heating. Nature 463:218–222

Boos WR, Kuang ZM (2013) Sensitivity of the South Asian monsoon to elevated and non-elevated heating. Sci Rep 3:1192. https://doi.org/10.1038/srep01192

Briegleb BP, Bitz CM, Hunke EC et al (2004) Scientific description of the sea ice component in the community climate system model, version three. NCAR Tech. Note NCAR/TN–463 + STR, 70

Charney JG, Eliassen A (1949) A numerical method for predicting the perturbation of the middle latitude westerlies. Tellus 1:38–55

Collins WD, Bitz CM, Blackmon ML et al (2006) The community climate system model version 3 (CCSM3). J Clim 19:2122–2143

Dee DP, Uppala SM, Simmons AJ et al (2011) The ERA-interim reanalysis: configuration and performance of the data assimilation system. Q J R Meteorol Soc 137:553–597. https://doi.org/10.1002/qj.828

Duan AM, Wu GX (2005) Role of the tibetan plateau thermal forcing in the summer climate patterns over subtropical Asia. Clim Dyn 24:793–807. https://doi.org/10.1007/s00382-004-0488-8

Flohn H (1957) Large-scale aspects of the summer monsoon in south and east Asia. J Meteorol Soc Jpn 35:180–186

Hahn DG, Manabe S (1975) The role of mountains in the South Asian monsoon circulation. J Atmos Sci 32:1515–1541

He ZQ, Wu RG (2013) Coupled seasonal variability in the South China Sea. J Oceanogr 69:57–69

He B, Wu GX, Liu YM, Bao Q (2015) Astronomical and hydrological perspective of mountain impacts on the Asian summer monsoon. Sci Rep 5:17586. https://doi.org/10.1038/srep17586

Held IM, Hou AY (1980) Nonlinear axially symmetric circulations in a nearly inviscid atmosphere. J Atmos Sci 37:515–533

Held IM, Ting M, Wang H (2002) Northern winter stationary waves: theory and modeling. J Clim 15:2125–2144

Hsu HH, Liu X (2003) Relationship between the Tibetan Plateau heating and East Asian summer monsoon rainfall. Geophys Res Lett 30(20):2066. https://doi.org/10.1029/2003GL017909

Huang R (1985) The influence of the heat source anomaly over Tibetan Plateau on the northern hemispheric circulation. Acta Meteorol Sin 43(2):208–220

Kawamura (1998) A possible mechanism of the Asian summer monsoon-ENSO coupling. J Meteorol Soc Jpn 76(6):1009–1027

Kitoh A (1997) Mountain uplift and surface temperature changes. Geophy Res Lett 24(2):185–188

Kitoh A (2004) Effects of mountain uplift on East Asian summer climate investigated by a coupled atmosphere–ocean GCM. J Clim 17(4):783–802

Kitoh A, Motoi T, Arakawa O (2010) Climate modeling study on mountain uplift and Asian monsoon evolution. Geol Soc Spec Publ 342:293–301

Koseki S, Watanabe M, Kimoto M (2008) Role of the midlatitude air–sea interaction in orographically forced climate. J Meteorol Soc Jpn 86(2):335–351

Lin PF, Liu HL, Zhang XH (2007) Sensitivity of the upper ocean temperature and circulation in the Equatorial Pacific to solar radiation penetration due to phytoplankton. Adv Atmos Sci 24(5):765–780

Lin PF, Liu HL, Yu YQ, Zhang XH (2011) Response of sea surface temperature to chlorophyll-*a* concentration in the Tropical Pacific: annual mean, seasonal cycle, and interannual variability. Adv Atmos Sci 28(3):492–510

Liu YM, Hoskins BJ, Blackburn M (2007) Impact of Tibetan orography and heating on the summer flow over Asia. J Meteorol Soc Japan 85B:1–19

Liu YM, Wu GX, Hong JL et al (2012) Revisiting Asian monsoon formation and change associated with Tibetan Plateau forcing: II. change. Clim Dyn 39:1183–1195

Liu HL, Lin PF, Yu YQ, Zhang XH (2013) The baseline evaluation of LASG/IAP climate system ocean model (LICOM) version 2. Acta Meteorol Sin 26(3):318–329. https://doi.org/10.1007/s13351-012-0305-y

Ma D, Boos W, Kuang Z (2014) Effects of orography and surface heat fluxes on the south asian summer monsoon. J Clim 27:6647–6659

Manabe S, Terpstra TB (1974) The effects of mountains on the general circulation of the atmosphere as identified by numerical experiments. J Atmos Sci 31(1):3–42

Montégut DB, Madec CG, Fischer AS, Lazar A, Iudicone D (2004) Mixed layer depth over the global ocean: An examination of profile data and a profile-based climatology. J Geophys Res 109:C12003. https://doi.org/10.1029/2004JC002378

Okajima H, Xie SP (2007) Orographic effects on the northwestern Pacific monsoon: role of air–sea interaction. Geophys Res Lett 34:L21708

Oleson KW, Dai Y, Bonan G et al (2004) Technical description of the community land model (CLM). NCAR/TN–461 + STR, 173

Paulson CA, Simpson JJ (1977) Irradiance measurements in the upper ocean. J Phys Oceanogr 7:952–956

Queney P (1948) The problem of air flow over mountains: a summary of theoretical studies. Bull Am Meteorol Soc 29:16–29

Saji NH, Goswami BN, Vinayachandran PN, Yamagata T (1999) A dipole mode in the tropical Indian Ocean. Nature 401:360–363

Schneider EK (1977) Axially symmetric steady–state models of the basic state for instability and climate studies. Part II: nonlinear calculations. J Atmos Sci 34:280–296

Schneider EK (1987) A simplified model of the modified Hadley circulation. J Atmos Sci 44(22):3311–3328

Schneider EK, Lindzen RS (1977) Axially symmetric steady–state models of the basic state for instability and climate studies. Part I: linearized calculations. J Atmos Sci 34(2):263–279

Tao SY, Ding YH (1981) Observational evidence of the influence of the Qinghai–Xizang (Tibet) Plateau on the occurrence of heavy rain and severe convective storms in China. Bull Am Meteorol Soc 62:23–30

Wang B, Bao Q, Hoskins B, Wu G, Liu Y (2008) Tibetan Plateau warming and precipitation changes in East Asia. Geophys Res Lett 35:L14702. https://doi.org/10.1029/2008GL034330

Wang ZQ, Duan AM, Yang S (2018) Potential regulation on the climatic effect of Tibetan Plateau heating by tropical air–sea coupling in regional models. Clim Dyn. https://doi.org/10.1007/s00382-018-4218-z

Wu GX, Zhang YS (1998) Tibetan Plateau forcing and the situating and timing of the Asian monsoon onset. Mon Wea Rev 126:913–927

Wu GX, Liu H, Zhao YC (1996) A nine-layer atmospheric general circulation model and its performance. Adv Atmos Sci 13:1–18

Wu GX, Li WP, Guo H, Liu H et al (1997) Sensible heat driven air–pump over the Tibetan Plateau and its impacts on the Asian Summer Monsoon. In: Collections on the memory of. Zhao J, Ye DZ (eds), Chinese Science Press, Beijing

Wu GX, Liu YM, Zhang Q et al (2007) The influence of the mechanical and thermal forcing of the Tibetan Plateau on the Asian climate. J Hydrometeorol 8:770–789

Wu GX, Liu YM, Dong BW et al (2012a) Revisiting Asian monsoon formation and change associated with Tibetan Plateau forcing: I. Formation. Clim Dyn 39:1169–1181

Wu GX, Liu YM, He B, Bao Q, Duan AM, Jin FF (2012b) Thermal controls on the Asian summer monsoon. Sci Rep 2:404. https://doi.org/10.1038/srep00404

Wu GX, He B, Liu YM, Bao Q, Ren RC (2015) Location and variation of the summertime upper–troposphere temperature maximum over South Asia. Clim Dyn 45:2757–2774. https://doi.org/10.1007/s00382-015-2506-4

Xu ZF, Fu CB, Qian YF (2009) Relative roles of land–sea distribution and orography in Asian monsoon intensity. J Atmos Sci 66:2714–2729

Xu ZF, Qian YF, Fu CB (2010) The role of land–sea distribution and orography in the Asian monsoon. Part II: Orography. Adv Atmos Sci 27(3):528–542

Ye DZ, Gao YX (1979) Meteorology of the Qinghai–Xizang Plateau. Chinese Science Press, Beijing, 278 **(in Chinese)**

Yeh TG (1950) The circulation of the high troposphere over China in the winter of 1945–1946. Tellus 2(3):173–183

Yeh TC, Luo SW, Chu PC (1957) The wind structure and heat balance in the lower troposphere over Tibetan Plateau and its surrounding. Acta Meteorol Sin 28:108–121

Zhao P, Chen LX (2001) Interannual variability of atmospheric heat source/sink over the Qinghai–Xizang (Tibetan) Plateau and its relation to circulation. Adv Atmos Sci 18:106–116

Zhou XJ, Zhao P, Chen JM, Chen LX, Li WL (2009) Impacts of thermodynamic processes over the Tibetan Plateau on the Northern Hemispheric climate. Earth Sci 39:1473–1486. https://doi.org/10.1007/s11430-009-0194-9